An Airborne Laser Air Motion Sensing System. Part I: Concept and Preliminary Experiment

R. J. KEELER, R. J. SERAFIN, R. L. SCHWIESOW AND D. H. LENSCHOW

National Center for Atmospheric Research, Boulder, CO*

J. M. VAUGHAN

Royal Signals and Radar Establishment, Gt. Malvern, UK

A. A. WOODFIELD

Royal Aircraft Establishment, Bedford, UK

(Manuscript received 18 February 1986, in final form 21 July 1986)

ABSTRACT

Measurement of air motion relative to an aircraft by a conically scanned optical Doppler technique has advantages over measurements with conventional gust probes for many applications. Advantages of the laser air motion sensing technique described here include calibration based on physical constants rather than experiment for an accurate measurement of mean wind, freedom from flow distortion effects on turbulence measurements, all-weather performance, reduction in error from mechanical vibrations and ability to measure vertical wind shear. An experiment comparing a single-component laser velocimeter and a differential pressure gust probe shows that the optical approach measures the turbulence spectrum accurately at frequencies up to 10 Hz and that the signal-to-noise ratio is not a limiting factor. In addition, we have observed the effect of spectral skewing caused by airflow distortion in cloud.

1. Scope and background

a. Intent and organization

This paper presents a concept for a laser air motion sensing system—a conically scanning Doppler velocimeter—that senses air motions remote from the aircraft, and it also presents results from a preliminary (one-component) feasibility experiment. The research was prompted by a recognition of the need for improved air motion sensing and is based on a laser Doppler scattering technique. Before performing a feasibility experiment, we analyzed the optical performance of a representative system to see if such an experiment would be worthwhile. It was. The experiment verified aspects of the sensing concept including operation of an airborne laser air motion sensing system with a small, closely focused sample volume and freedom from unexpected problems such as vibration. We had intended for an experiment to verify the complete concept, but a laser air motion sensing system with the required scanning capability is not yet available.

Our purpose is to document the concept and feasibility of the air motion sensing system for evaluation by the research community. Although the verification experiment did not involve scanning, this report may be useful to others contemplating related research and evaluating other laser air motion sensing configurations. Because the research followed the order of concept, analysis and experiment, we retain that order for clarity in the presentation.

The context of our research includes Keeler and Serafin (1983), who originally proposed the optical technique for air turbulence measurements that is discussed here in more detail. The success of the verification experiment showed that more detailed analysis of the performance of the scanning configuration was in order. In the companion paper, Kristensen and Lenschow (1986) show theoretically that the conically scanning technique can resolve the three wind component spectra to wavelengths as small as 40 m and can resolve eddy structures for flux measurements at wavelengths of 100 m when the range to the sample volume is 10 m.

Basically the technique proposed here relies on the measurement of the relative motion of aerosol particles by their Doppler shift using a laser mounted on the aircraft. For various practical and technical reasons, a CO_2 laser operating near 10.6-μm wavelength in the middle infrared is a good choice for the source. Scat-

* The National Center for Atmospheric Research is sponsored by the National Science Foundation.

tering at this wavelength is predominantly by particles of 1- to 3-μm radius (Post, 1978).

b. Scientific needs for improved air motion sensing

One of the most important and difficult measurements to obtain from aircraft is wind velocity. Since the aircraft speed typically is an order of magnitude greater than the horizontal wind, estimating the wind component along the aircraft heading involves calculating small differences between large numbers—basically the difference between the aircraft's true airspeed and ground speed. The wind components normal to the aircraft heading are calculated in existing systems from the airflow angles, the airspeed, the airplane attitude angles and the velocity of the aircraft. All of these variables must be measured accurately in order to obtain the air motions. At a speed of 100 m s^{-1}, for example, a change in flow angle of only 1° is equivalent to a 1.7 m s^{-1} change in the transverse wind component in the plane of the angle change.

As discussed by Lenschow (1986), there are many sources of error in wind measurements from aircraft. In the past, one of these has been the accuracy with which the airplane velocity can be measured. Presently used inertial navigation systems have typical drift rates of $\sim$0.5 (m s^{-1})h^{-1}. This can be reduced considerably now with radio navigation or other independent systems. Before the end of the decade, aircraft navigation may be revolutionized by satellite-based radio navigation, which promises 3-dimensional position accuracy of <20 m and velocity accuracy of <0.1 m s^{-1} (Parkinson and Gilbert, 1983).

The error caused by flow distortion induced by the aircraft and its appendages (Wyngaard et al., 1985) is a more fundamental limitation in present wind measurement techniques that use vanes or pressure ports immersed in the airflow. In designing existing airborne air motion sensing systems, a compromise has to be made between the requirements to make the air motion measurements as far away from the airplane as possible, and yet maintain a structurally sound linkage between the air velocity sensors and the airframe. The trade-off between these requirements has led to the use of booms that extend approximately a fuselage diameter from the nose of the aircraft. The result is that even if the flow angles can be resolved to a fraction of a degree, and the airspeed to a few centimeters per second, the errors from flow distortion are likely to be considerably greater than this. Virtually all immersion sensing techniques have a flow distortion problem; it can be particularly severe with aircraft because of their speed.

In practice, the effects of flow distortion on specific instruments have usually been estimated by flight maneuvers (e.g., Lenschow, 1985) although numerical calculations may be a viable alternative. In either case, corrections are not accurate enough to allow measurement of the mean vertical wind component, which is severely limited also by the capability of the inertial navagation system; furthermore, the mean horizontal wind components probably cannot be measured consistently to much better than approximately one meter per second. Yet, there are many meteorological problems that require better wind accuracy. For example, measurements of mesoscale phenomena such as flow patterns in prestorm environments, land–sea breeze circulations and orographic flows require horizontal and vertical absolute wind measurements with an accuracy of a few tenths of a meter per second.

Wyngaard et al. (1985) also point out that even if the mean winds could be corrected for flow distortion effects, turbulence statistics can still be in error. This problem becomes apparent when calculating the covariances of two velocity components, such as $\overline{u'w'}$, and can lead to significant errors in the measured turbulence stress. The problem is important because covariance measurements from aircraft are useful in many applications. Vertical turbulence fluxes, which are covariances of vertical velocity with other colocated variables such as temperature, humidity and trace gas concentrations, are essential in quantitative studies of boundary layer and cloud dynamics, and of transport and transformations of trace atmospheric constituents. In order to measure all the significant contributions to the turbulence flux in a convective boundary layer, spatial wavelengths at least as small as 100 m must be resolved to sense at least 80% of the turbulence flux at altitudes of 35 m or greater (Caughey and Kaimal, 1977).

Airflow measurements using the deflection or strain of vanes and using pressure differentials (Pitot tubes and differential-pressure angle sensors) employ transducers that require frequent recalibration. In addition, the relation between air motion and pressure or force angle measurements depends in a complex way on flow around the aircraft, which can be changed by the addition of other sensors on a research aircraft, and on air density. Often a final empirical calibration is performed by calculating the wind for reciprocal flight tracks and determining a correction factor.

Problems with present air motion sensors, the improved accuracy soon possible in airplane ground speed measurements using a global positioning system, and evolving scientific needs for more accurate air motion measurements all point to the desirability of improving air velocity instrumentation. The improved technique should measure air velocity remote from the aircraft, yet close enough that the coherence between the remotely measured velocity and the velocity at the point where scalar variables are measured is still high at wavelengths that are important for turbulent transport. Furthermore, the technique should also be able to resolve the velocity component spectra at wavelengths at least as small as 40 m with an absolute accuracy of 0.1 m s^{-1}, and operate in any kind of weather encountered by the aircraft—most notably within clouds and precipitation.

In summary, the advantages of the laser air motion sensor compared to presently used vanes and pressure-difference techniques are

1) accurate absolute wind measurements,
2) minimal flow distortion effects on mean and turbulence values,
3) operation in precipitation and clouds,
4) no mechanical resonance effects (no boom), and
5) ability to measure vertical wind shear (Kristensen and Lenschow, 1986).

c. *Relation to other work*

To sense relative air motion, the optical system should operate at only one range but must measure all three components of the relative air motion with high spatial and temporal resolution. Other optical Doppler remote velocity sensors display different measurement characteristics.

Muñoz et al. (1974) conducted early work to measure the true airspeed of an aircraft with an optical Doppler system to avoid the problem of flow interference caused by an aircraft's fuselage. This work showed the feasibility of obtaining airspeed, but measurements of turbulence spectra and comparison with other types of sensors were not attempted.

Cannell et al. (1983) and Woodfield and Vaughan (1983) used more modern optical equipment to measure true airspeed, with an emphasis on detecting wind shear by sensing the relative air motion of a long, narrow volume 300 m ahead of the aircraft. In this application the Doppler unit served as a predictive airspeed and turbulence indicator, but its spatial resolution was inadequate for fine-scale turbulence measurements. Keeler and Serafin (1983) in their oral presentation at the Second Topical Meeting on Coherent Laser Radar gave theoretical evidence that the signal-to-noise ratio of a system like that used by Cannell et al. would be adequate for high-frequency and high-resolution measurements. Keeler et al. (1984) orally presented preliminary results using the laser airspeed indicator to measure one component of the relative air motion in this high-resolution mode.

In contrast to laser airspeed indicators, a laser air motion sensing system measures three components of the relative air motion at a virtual point colocated with other turbulence measurements for use in covariance calculations. By colocated, we mean that the air motion measurements are made close enough to the aircraft and with high enough spatial resolution that conventional techniques for temperature, humidity, etc. can be used together with a time lag correction and a frozen flow hypothesis over the 40-m averaging lengths (Kristensen and Lenschow, 1986) characteristic of the air motion measurement technique. Of course, remote techniques for other atmospheric variables are ideally suited, but not necessary, for combination with the laser air motion sensor. Accurate relative air motion measurement combined with measurement of aircraft velocity and angular orientation yields measurement of the air velocity with respect to the earth. The laser air motion sensor differs from a laser airspeed indicator in operating range, spatial resolution and number of components measured.

Airborne pulsed Doppler lidars differ from gust probes in that the emphasis of the former is on remote mapping of the atmospheric wind field rather than on in situ measurements near an aircraft, but the technology is relevant to our study. Both cw (Schwiesow et al., 1981a) and pulsed (Bilbro et al., 1984; Eilts, et al., 1984) airborne Doppler lidars have been used for various types of studies. Dickson and Ottesen (1980) mounted a lidar using a forward conical scan on a helicopter to measure downwash velocity at ranges of 1–60 m from the lidar. Against this background it is clear that a laser air motion sensor represents an evolution of existing airborne remote sensing capability rather than an unproven technique.

2. Laser air motion sensor concept

a. *Geometry and uncertainty*

1) THREE-COMPONENT MEASUREMENTS

An optical Doppler sensor measures the component of the relative motion between the source and scatterer along the optical axis (the radial component) with a range-dependent weighting function that is peaked at some distance from the instrument. Although it is a cw device, it is a true remote sensor with the sensing volume topologically separated from the sensor. To obtain all three components of the relative velocity, measurements at multiple angles are needed. One way to do this is to set the optical beam at an angle to the aircraft's longitudinal axis and rotate the beam about the axis, as proposed by Keeler and Serafin (1983). The beam scan generates a cone with respect to the aircraft, and the sensing volume of the Doppler velocimeter follows a helix in space. Kristensen and Lenschow (1986) in the companion paper show details of the geometry involved. Conical scanning is commonly used in ground-based radars and lidars to obtain three components of the wind (e.g., Lhermitte and Atlas, 1961; Browning and Wexler, 1968) and need not be analyzed here. Alternate approaches might use three separate scan angles or simultaneous multiple beams; the analysis is similar in either case. Multiple beams intersecting at a point ahead of the aircraft (Schwiesow et al., 1977) is another possible geometry that could yield higher spatial resolution.

Kristensen and Lenschow (1986) produced the intuitively satisfying result that a cone half-angle of approximately 45 deg gives the best estimate of the three velocity components for determination of turbulence spectra. This is because at the cone half-angle limit of 0 deg, the Doppler sensor measures the longitudinal

component well and the transverse components not at all, and at the limit of 90 deg it measures only the transverse components. Assuming a range of 10 m to the sample volume to minimize the flow distortion caused by the fuselage, the region of the atmosphere sampled is approximately 15 m in the transverse direction. With this separation, the laser air motion sensor can resolve velocity spectra with spatial wavelengths as small as 40 m and eddy structure to wavelengths of 100 m (Kristensen and Lenschow, 1986).

To convert from measured Doppler frequency shift to relative velocity requires knowledge of only the laser wavelength and the speed of light. In contrast to presently used gust probes, the measurement of the radial component of the velocity requires no experimental airflow calibration and contains negligible systematic (i.e., bias) error. The only uncertainty arises from the fact that the Doppler signal comes generally from a number of scatterers in the sample volume, each of which may have a slightly different radial velocity component, and the fact that the optical system measures the radial component over a narrow range of ray angles determined by beam convergence. As a result, the Doppler signal has a spectrum with finite spectral width containing contributions from atmospheric effects and from the geometry of the optics, as well as from the spectrum analysis process. In the sense that the Doppler spectrum is made up of returns from many scatterers, it can be thought of as an intensity-weighted histogram or probability density function of the velocities within the scattering volume. The uncertainty of the velocity estimate is simply the random error associated with determining the mean of the Doppler spectrum.

2) DOPPLER SPECTRUM VS VELOCITY SPECTRUM

It is important to understand the difference between the concepts of a Doppler spectrum as used in remote sensing and the velocity spectrum derived, for example, from an in situ, single-point measurement of the time series of velocity. Although both kinds of spectra are based on the variation in the wind field, a Doppler spectrum comes from the summation of signals from different scatterers in the total sample volume, but the velocity spectrum comes from analysis of the time series of velocity estimates as would be made, for example, with a single-axis sonic anemometer (where the mean wind advects the field by the sensor) or with an airborne laser velocimeter (where the aircraft moves the sensor through the field). A Doppler spectrum represents the distribution of velocities in the sample volume and may be obtained in a short integration time (e.g., 50 μs), whereas a velocity spectrum requires a time series obtained over a longer time (e.g., 10 s), that depends on the lowest frequency of interest. To obtain a velocity spectrum from a Doppler velocimeter, the Doppler spectrum is processed to give a single velocity estimate for a suitable integration time by calculating either the mean of the spectral distribution or some other frequency estimator, such as the peak of the spectrum. The time series of these velocity estimates can then be analyzed to produce a velocity spectrum in the same way as is done with conventional anemometers.

Note that the difference between the time series of velocity values produced from a collection of point measurements and that produced from measurements by a remote sensor that averages over a finite spatial volume is one of degree. No sensor can make a true point measurement, but the sampled volumes for conventional in situ sensors tend to be smaller than those for most remote sensing devices.

3) VELOCITY UNCERTAINTY

The uncertainty in the velocity estimated from a Doppler spectrum depends on the Doppler spectrum width, the signal-to-noise ratio (SNR) and the averaging time. Keeler (1980) compares errors in Doppler velocity estimates made from simulated lidar data with the calculations of Zrnic' (1979) for expected errors in velocity estimates as a function of SNR for various Doppler spectrum widths and averaging times. Keeler found that expected errors are similar for data processing algorithms using either Fourier analysis or a single-lag covariance estimator. Zrnić (1979) predicts, and Keeler (1980) confirms, that for high SNR (>20 dB at the detector output) the radial velocity uncertainty is

$$\epsilon = (\lambda s/8\pi^{1/2}T)^{1/2} \quad (1)$$

where λ is the laser wavelength, s the standard deviation of the Doppler spectrum (the $1-\sigma$ width or approximately one-half the full width at half maximum), and T the integration time, which must be several times the coherence time of the signal. For SNRs near 0 dB, the typical uncertainty is approximately three times larger. If N independent velocity estimates, each with the same uncertainty, are averaged, the uncertainty in the average is smaller than the individual uncertainty by a factor $1/N^{1/2}$.

The data shown later from this experiment have spectral widths of 1 m s^{-1} or less and large SNRs. A surface-acoustic-wave spectrum analyzer with an integration time of 25 μs was used in the present experiment to produce the Doppler spectra. With these values, the expected uncertainty from (1) is $\epsilon = 0.17$ m s^{-1} for a velocity estimate from a single spectrum. An on-board processor averaged 100 such spectra before making a velocity estimate, so the velocity time-series results with an integration time of 2.5 ms (100 times 25 μs) have an expected measurement uncertainty of approximately ± 0.02 m s^{-1}. Actual fluctuating velocities apparently mask these small random measurement uncertainties. It is easy to estimate the standard deviation (i.e., the $1-\sigma$ spectral width) from the experi-

mental data, but we do not have an independent measurement of the radial velocity component at the velocimeter sample volume. Without an independent estimate, it is not possible to verify the expected uncertainty as a rms difference between two simultaneous measurements.

We may obtain an independent estimate of the velocity uncertainty from Lee and Lee (1980), who discuss a lidar simulation using a multiple-lag covariance frequency estimator. For a CO_2 Doppler lidar return with a spectrum width of 0.5 m s^{-1} and integration time of 6.8 μs (a range gate of 1 km for a pulsed system), they find an uncertainty of less than 0.2 m s^{-1} for a velocity estimate based on a single pulse (i.e., single estimate) with high SNR. The assumed conditions are similar to those in our experiment, so we conclude that the estimates from (1) are reasonable.

Although it is comparatively easy to determine the uncertainty in the measurement of the radial component of the velocity, it is much more difficult to analyze how well a conical scan estimates all three components of the relative velocity. Because a large number of radial velocity estimates around the conical scan contribute to the estimate of the three components of the relative motion, these values will be subject to a statistical uncertainty that is related to, but smaller than, the radial velocity component uncertainty. However, in addition to uncertainty from measurement statistics, the spatial variability of the turbulence introduces an uncertainty in determining the three components of the wind field at a point on the longitudinal axis of the aircraft because velocity measurements are made along a helical trajectory around the longitudinal axis. Kristensen and Lenschow (1986) examine these effects on estimation of the atmospheric turbulence spectrum.

b. Signal-to-noise ratio

Although the signal-to-noise ratio (SNR) in a heterodyne, cw lidar has been previously documented in various places (e.g., Foord et al., 1983), there exist significant differences in interpretation between scientists with optical and radar backgrounds. The tutorial review in this section is intended to aid in reconciling different viewpoints, with a particular emphasis on the square-root dependence of SNR on received optical power, characteristic of photon statistics, and the linear dependence, characteristic of radar detector output. Similarly, the bandwidth over which noise is measured requires careful definition as either the reciprocal of the measurement time, characteristic of photon counting, or the total bandwidth of the Doppler processor, as used in radar. Noise can be either the fluctuations on the no-signal baseline, used in optical heterodyning, or the total (constant plus fluctuating) detected power, as in radar.

In the context of this research, the motivation for considering the SNR expected from a laser air motion sensor is threefold. First, we use SNR as an aid in understanding the operation and performance of such a device and the choice of certain design parameters. Second, a large SNR is necessary to justify the velocity uncertainty calculated in (1). Third, we need to establish a quantitative framework to evaluate the experimental results reported later and check on our understanding of the instrument and its performance. Keeler et al. (1984) showed preliminary evidence to support an expectation of SNRs > 10 dB in the boundary layer.

1) BACKSCATTER COEFFICIENTS

Although much research on the climatology of aerosol backscatter coefficient profiles at 10.6 μm wavelength remains to be done, Post (1984) presents some of the best available statistics for continental air masses. The backscatter coefficients tend to follow a lognormal distribution for any particular season and altitude. For example, typical values at 4 km above sea level range from 7×10^{-10} m^{-1} sr^{-1} in winter to 7×10^{-9} m^{-1} sr^{-1} in the summer, so a representative value is near 2×10^{-9} m^{-1} sr^{-1} at the 50% probability level. The standard deviation is approximately a factor of five times the mean at this altitude and somewhat greater in the boundary layer. In the boundary layer the backscatter coefficient is near 1×10^{-8} m^{-1} sr^{-1} (e.g., Schwiesow et al., 1981b) at 10.6-μm wavelength.

2) PERFORMANCE CALCULATIONS

The received signal power for a focused cw optical backscatter system is independent of range and optical aperture for all focal distances (i.e., weighting function peaks) shorter than that corresponding to the infinity focus point of the telescope (approximately the square of the telescope aperture divided by four times the wavelength) of the system. The optical power incident on the receiver telescope in this case (e.g., Schwiesow, 1986) is given by

$$P_s = 2\pi\lambda\beta P_t \tag{2}$$

where β is the backscatter coefficient, λ the optical wavelength, P_t the transmitted power, and the geometrical factors vary depending on the definition of scattering length for a focused cw system. The scattering length depends on the aperture illumination and is given approximately by $1 = 8.5\lambda(R/D)^2$, and the diameter of the scattering volume is approximately $d = 2.44\lambda R/D$ to the first minimum of the Airy diffraction pattern, where R is the range to the focal volume and D is the telescope aperture diameter. The photon arrival rate is simply

$$R = P_s/h\nu, \tag{3}$$

where ν is the optical frequency ($\nu = c/\lambda$) and h is Planck's constant. We have assumed the atmospheric transmission to be 1 and neglected a number of optical efficiency factors discussed in detail by Foord et al. (1983).

For the direct detection of arriving photons (photon counting) in the ideal case of minimum noise, where the noise is dominated by statistics on the photon arrival rate (i.e., the signal fluctuations are shot noise only, with negligible background and detector noise), the SNR is easy to calculate by standard methods (e.g., Foord et al., 1983, or Schwiesow, 1986). There are different definitions of SNR in use, and comparing results in the literature requires proper conversions to be made. The total number of photons incident on the receiver is R times T, where T is the integration (photon-counting) time and the reciprocal of the measurement bandwidth $b = 1/T$. If we define "noise" as the uncertainty in estimating the "signal", which is defined as the true photon arrival rate R^* from a measurement over T, then Poisson statistics gives the fundamental optical SNR in the received beam as (Boyd, 1983)

$$(\mathrm{SNR})_{opt} = (RT)^{1/2} = (P_s/h\nu b)^{1/2}. \quad (4)$$

In other words, the fundamental noise is the rms fluctuation in the photon arrival rate from a constant source.

Because a photon generates a charge carrier in the detector with some probability (quantum efficiency) η, the detector signal current i_s is proportional to the optical power in the received beam. The total charge transferred in the detector in time T is

$$Ti_s = eRT\eta, \quad (5)$$

and the fluctuation in the charge (uncertainty in estimating the true rate) leads to a noise current i_n given by

$$Ti_n = e(RT\eta)^{1/2}, \quad (6)$$

where e is the carrier charge. The SNR for the electrical power at the output of the detector for direct photon detection is the ratio of the *squared* currents in (5) and (6) as

$$(\mathrm{SNR})_{det} = RT\eta = \eta P_s/h\nu b. \quad (7)$$

Thus, the SNR at the detector output is the detector quantum efficiency times the square of the fundamental SNR determined by photon statistics, because detector current is proportional to optical power (i.e., to photon arrival rate).

Shot-noise-limited detection is typical also of well-designed lidar systems that use heterodyne detection. An analysis similar to but more complicated than that for direct detection can be applied to heterodyne detection (e.g., Yariv, 1985; Boyd, 1983), and leads to an expression identical to (7) for the SNR at the heterodyne detector output when the local oscillator power is large enough that the performance is limited by shot noise from the local oscillator. Note that the local oscillator power level does not appear in (7), even for the heterodyne case. From this we conclude that the limiting SNR is the same in the heterodyne case as in the photon counting case; both are limited by Poisson statistics, although photon counting and thus direct observation of SNR_{opt} is not feasible with heterodyning.

In the optical heterodyne case, the local oscillator causes a large detector current, even in the absence of any atmospheric scattering signal. Signal power may be represented as the integral of the power spectrum that is above the average local oscillator baseline, and noise power, as the fluctuations on the baseline, which are a result of shot noise from the local oscillator integrated over the same bandwidth as the signal (Foord et al., 1983). In practice, both signal and noise are measured with a radio frequency filter bank or spectrum analyzer.

The inherent bandwidth of the optical signal is approximately equal to the reciprocal of twice the atmospheric coherence time measured at the $1/e$ point on the correlation function. This coherence time is

$$\tau = 2^{1/2}\lambda/4\pi s \quad (8)$$

(Gossard and Strauch, 1983). For a velocity spread s = 1 m s^{-1} and a lidar at 10.6 μm, the $1/e$ coherence time is approximately 1.2 μs. The signal bandwidth for this typical case is 1/(2.4 μs) or approximately 420 kHz. When the integration time of the analyzing instrument is longer than twice the atmospheric coherence time, the signal bandwidth is appropriate for (7). In other words, the atmospheric coherence time sets the upper limit for the time over which coherent averaging of the signal is possible.

Because the Doppler spectra observed in the experiment were averages of many individual spectra, it is important to consider the SNR of spectra averaged incoherently. We may define the SNR for the average of N independent heterodyne measurements or spectra (i.e., postdetection averaging) as $N^{1/2}$ times the SNR in (7). We compare the predictions of (7), including averaging, with the experimental results later.

3. Single-component experiment

We performed an experiment in May, 1984 to test the concept of using an airborne Doppler velocimeter focused close to the aircraft to measure relative air motion. Although a scanning mechanism was not available, our judgment is that a comparison of one-component measurements made by the laser velocimeter and a conventional 5-port pressure-differential gust probe (similar to the Rosemont 858) provides a useful test of a laser system focused closer to the aircraft body than was the case for previous measurements (Woodfield and Vaughan, 1983).

a. Equipment

The Doppler velocimeter used in the experiment was mounted on an HS-125 twin jet aircraft operated by the Royal Aircraft Establishment from Bedford, England. The velocimeter was provided by the Royal Signals and Radar Establishment of Malvern, England,

and employs a cw, waveguide CO_2 laser, which operated at 2 W in the experiment. The transmitter beam is expanded to 10 cm at the $1/e$-squared intensity points. A surface-acoustic-wave (SAW) spectrum analyzer with 25-MHz bandwidth produces the Doppler spectra, which are summed in a high speed digital integrator. Spectral moment data are available at a rate of 20 s^{-1} and complete Doppler spectra at 10 s^{-1}. Cannell et al. (1983) and Foord et al. (1983) give more detail on the instrument.

For one comparison test, the axis of the optical system was at +1.7° to the aircraft axis, and the small, boom-mounted differential pressure gust probe was at −6.8° (to align with the streamlines at slow-test airspeeds). This alignment difference should introduce less than 0.5% difference in the airspeed readings on the two instruments. For a later test the optical axis was changed to −6.8°. In this preliminary experiment the velocimeter was not scanning; only the component of the relative air motion along the fixed axis of the optical system was measured. The boom was mounted above the axis of the nose cone with the probe extending approximately 1 m forward of the tip of the nose cone, where the velocimeter window was located. The shortest range at which the beam could be focused was 16 m ahead of the pressure probe, which provided a depth of focus of approximately 1.2 m.

b. *Time series data*

Figure 1 compares the longitudinal air motion component measured by the differential pressure probe and the optical probe over a time interval of 6 s. For comparison, pressure data taken at 256 s^{-1} were sampled at 25.6 s^{-1} in Fig. 1 to correspond to the 20 s^{-1} velocimeter data. Figure 2 has similar data on a different run for a longer time. One immediately obvious difference between pressure difference and optical data is that the pressure-determined airspeeds are low compared to the optically determined airspeeds, and that the difference varies between runs.

These airspeed differences emphasize the calibration simplicity advantage of the optical Doppler technique. The difference between the two airspeeds probably comes from inaccurate correction of the pressure data, although the possibility of a nonfundamental error in the spectral processing cannot be ruled out. The difference does not come from an uncertainty in the laser wavelength because the laser was rigidly locked to the P-20 line of the CO_2 molecular spectrum. The wavelength lock involves a narrowband interference filter in the local oscillator path with >70% transmission at P-20 and <10% for other lines, combined with an electronic feedback loop driving a piezoelectric translator on a laser cavity mirror. In addition, the low-pressure laser operated on a single longitudinal cavity mode, which assures a sufficiently narrow transmitter frequency, and the same laser served as transmitter and local oscillator (homodyne configuration), which assures that a zero optical beat frequency corresponded to zero relative radial velocity component. Airspeed data based on pressure differences must often be corrected by an empirical factor, determined by flying reciprocal headings in a presumed homogeneous atmo-

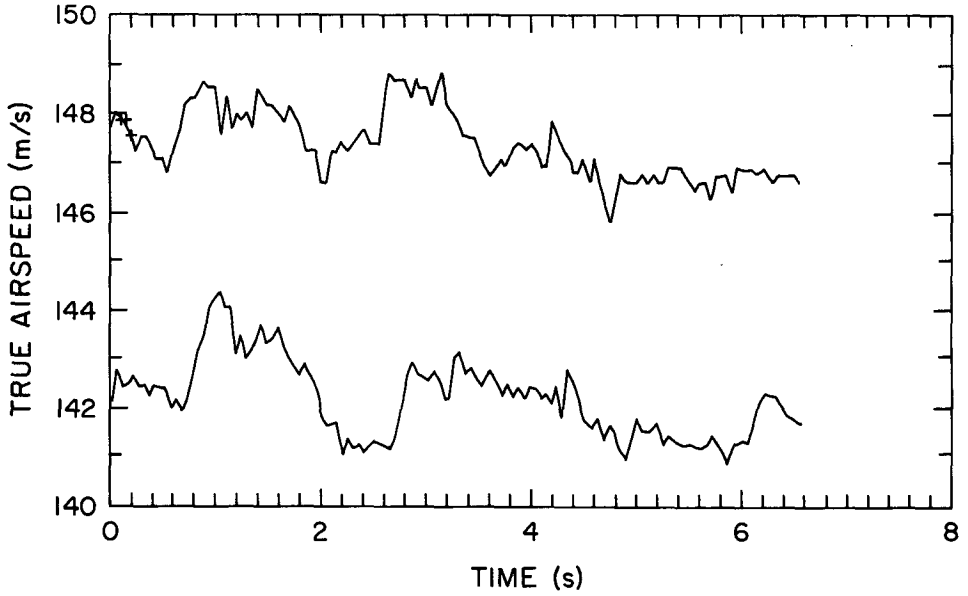

FIG. 1. Time series of the longitudinal component of relative air motion measured by an optical Doppler velocimeter focused 17 m ahead of the aircraft (top trace), and by a pressure-differential gust probe on a boom (bottom trace). The laser air motion sensor was sampled at 20 s^{-1}, and the pressure differential at 25.6 s^{-1}. The time offset is estimated as ~0.11 s, which corresponds to a focal distance 16 m ahead of the boom tip.

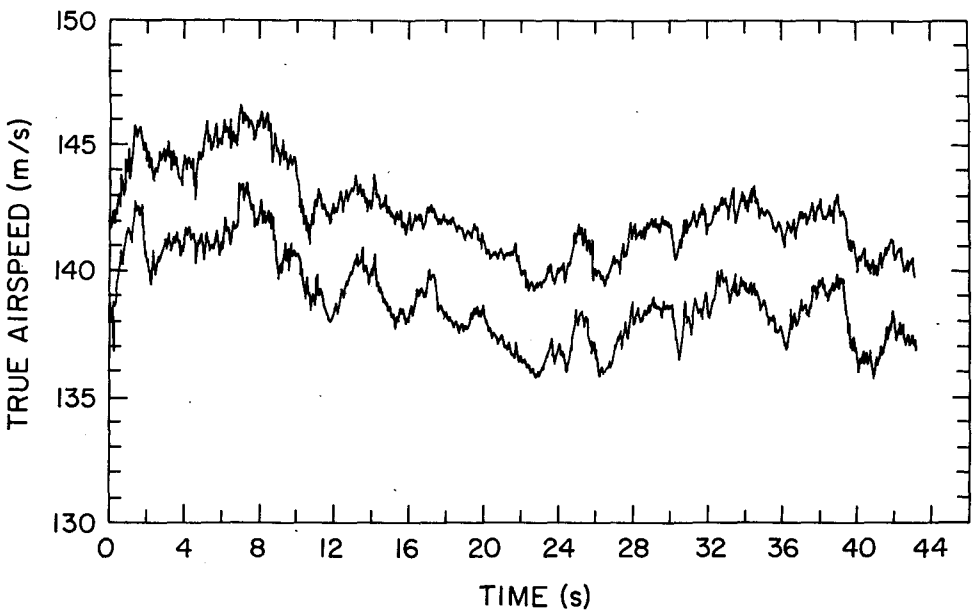

FIG. 2. As in Fig. 1 except for laser data sampled at 25 s^{-1}. The variance computed from the optical Doppler velocimeter data is 2.88 $(m\ s^{-1})^2$, and from the pressure-differential data is 2.89 $(m\ s^{-1})^2$. The time offset is ~0.11 s.

sphere and comparing the derived wind speeds (Lenschow, 1986). A reciprocal heading check was not part of the pressure difference airspeed analysis in this experiment.

1) TIME LAG

The optical data lead the pressure data in time, as expected, because the optical system is focused ahead of the aircraft. In Figs. 1 and 2 the lead is approximately 0.11 s for a focal distance 16 m ahead of the boom tip. In both cases, the airspeed traces are not simply time-shifted replicas of each other. Large-scale features of the time series, which we can subjectively estimate at approximately 1–4 s, tend to be observed in both traces, but smaller scale fluctuations are not identical in both records. Some of the difference in the small scale comes from the fact that the two instruments sense different air parcels when the optical beam is displaced laterally from the pressure probe; the amount of displacement (assuming a pitch angle of 6.8°) is roughly 2 m at 16 m range for the data in Fig. 1. The displacement for data in Fig. 2 was less. Kristensen and Jensen (1979) show that for isotropic turbulence with a frequency spectrum proportional to a −5/3 power law, the coherence between airspeeds measured with a lateral separation of 2 m decays to 0.5 at a frequency of 5 Hz. This seems to account qualitatively for some of the small-scale differences in the time series.

2) FREQUENCY RESPONSE

To compare the response of the two techniques to turbulence it is helpful to compare velocity spectra of the time series measurements. The dot–dashed reference lines in Figs. 3 and 4 are fixed at a −5/3 power law slope but the y-intercept is allowed to vary to fit the data. The pressure-difference turbulence data (not smoothed in this case) follow the −5/3 law up to approximately 80 Hz, after which they show greater power. This change in slope above 80 Hz is possibly the result of spectral aliasing or of measurement noise. Aliasing of the 400-Hz power-supply spike with a sampling rate of 256 s^{-1} occurs at 112 Hz, and its sidelobes contribute to the spectrum. The optical turbulence data in Fig. 4 follow the reference slope quite well up to the 10-Hz limit imposed by the data system. The significant differences between the two power spectra are the high-frequency cutoff and the power intercept of the fitted reference line, which is 3 dB lower for the optical data than for the pressure-difference data. The power intercept for the pressure-difference data is raised by the contribution from energy above 10 Hz in the spectrum; when the pressure data only up to 10 Hz are fitted, the power intercepts at 1 Hz for spectra measured by the two techniques are the same to two significant figures.

Spectra in Figs. 5 and 6 show the same features as those in Figs 3 and 4. Power intercepts in both cases are approximately the same for data up to 10 Hz. Velocity variances for the time series in Fig. 2 agree closely with each other. The variance (sigma-squared) for the laser velocimeter data is 2.876 $(m\ s^{-1})^2$, and for the pressure-difference probe is 2.893 $(m\ s^{-1})^2$.

We conclude that turbulence spectra measured by the one-dimensional laser air motion sensor are essentially the same as those measured by a conventional

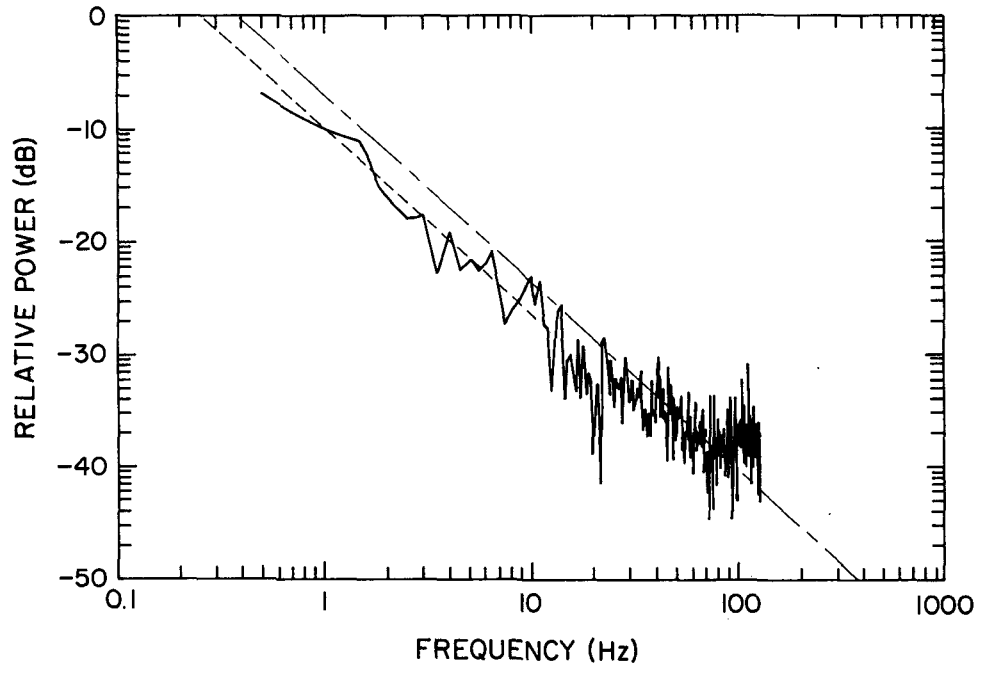

FIG. 3. Velocity power spectrum of the time series from which the pressure-differential data in Fig. 1 were derived, but sampled at the full 256 s^{-1} rate. The slope of the dot–dash line is fixed at −1.67 and the fitted y-intercept at 1 Hz is −6.97 dB. The y-intercept at 1 Hz of the dashed line fitted to the spectrum up to 10 Hz is approximately −10.27 dB.

pressure-difference gust probe up to approximately 10 Hz.

c. *Doppler spectra*

1) TURBULENCE

Atmospheric turbulence is revealed by fluctuations in the time series of velocity as discussed in subsection 3b(2). For a remote sensing technique that integrates over a weighted volume of the atmosphere, inhomogeneities in the wind field appear as a spread in the Doppler spectrum. (The Doppler spectrum is the sum over all scattering centers of the scattered power plotted at each value of the Doppler shift.) Figure 7 is a Doppler spectrum of the detector voltage, which is proportional to the square root of the electrical signal power, so the full spectrum width at half power (FWHP) is measured at 0.707 times the peak of the spectrum. For this spectrum the FWHP value is 1.5 m s^{-1}.

One contribution to the spectral width is the range of longitudinal velocity components present in the sample volume. However, effects other than turbulence are present and contribute to the width of the observed Doppler spectrum. The spectrum analyzer used in the experiment had a frequency resolution of 60 kHz, which corresponds to a velocity of approximately 0.3 m s^{-1}. This electronic instrumental broadening is convolved with the Doppler spectral width of the signal that results from atmospheric turbulence and the optical geometry. Contributions to the spectral width from the optical signal add in an rms fashion. A 15 cm optical aperture (10 cm $1/e$-squared points on the transmitted beam) working at a wavelength of 10.6 μm and a range of 16 m has a diffraction-limited depth of focus of approximately 1.2 m and a waist diameter of approximately 2.8 mm. At a measured true airspeed of 149 m s^{-1}, this longitudinal distance corresponds to a residence time of approximately 8.2 ms in the optical beam. The resulting broadening, less than 0.15 kHz, contributes less than 0.001 m s^{-1} to the spectral width. In the transverse direction, a particle crossing the beam at 2 m s^{-1} (vertical or sideslip component) will have a residence time of at least 1.4 ms. This would contribute a broadening of 0.004 m s^{-1}. If the beam were aligned at 6.8° to the streamlines, a scatterer would have a residence time of 0.16 ms at the beam waist, which leads to a broadening of 0.033 m s^{-1}. Another small contribution to the spectral width at 16 m range is the distribution of ray angles in the converging beam. The angle is 0 rad for the axial ray and 3.1 mrad for a marginal ray from the edge of a 10-cm diameter beam, and the departure of the cosine of this angle from 1 is less than 6×10^{-6}. Applying this to the 149 m s^{-1} airspeed results in a variation in radial component of less than 0.001 m s^{-1}. The video response of the display adds only slight broadening because the steps corresponding to individual analyzer channels can be seen

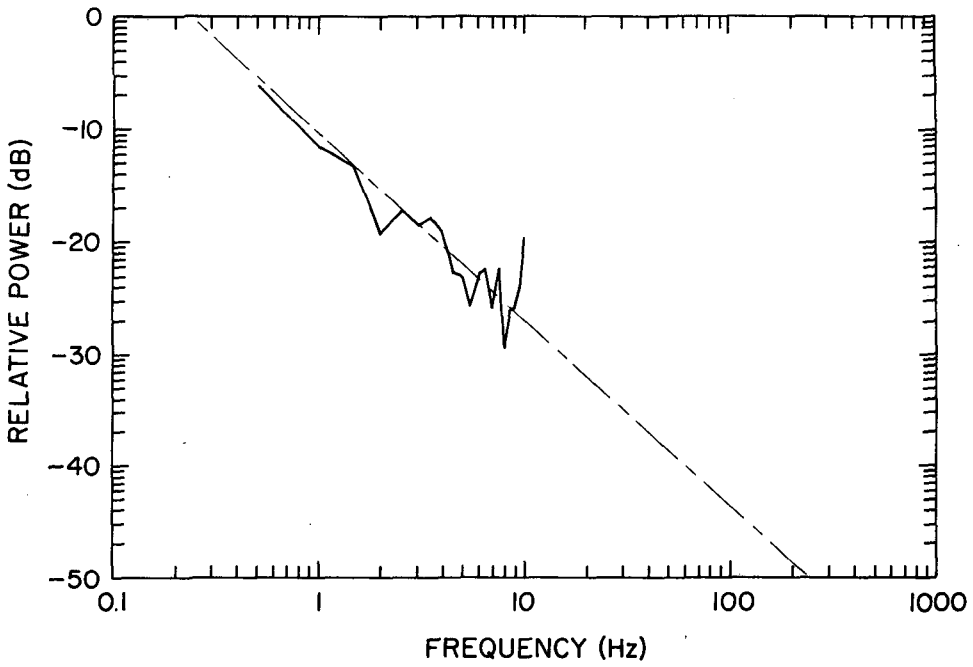

FIG. 4. Velocity power spectrum of the time series in Fig. 1 that is derived from laser velocimeter data. The fitted y-intercept at 1 Hz is -10.28 dB.

in the original of Fig. 7. Summing up, we can account for less than 0.1 m s^{-1} spectrum width from the optical geometry and 0.3 m s^{-1} from spectral processing.

Each Doppler spectrum is the average of data accumulated over less than 0.1 s, so the sample volume for a spectrum is at most 17 m (15 m flight path plus

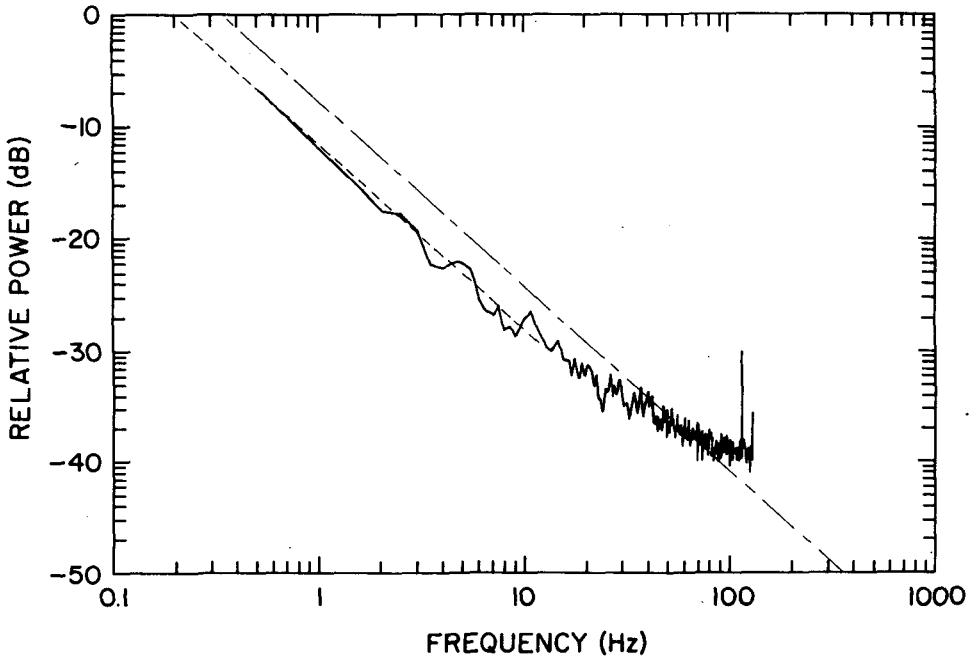

FIG. 5. Velocity power spectrum of the time series from which the pressure-differential data in Fig. 2 were derived, but sampled at the full 256 s^{-1} rate. The fitted y-intercept at 1 Hz to the dot–dash line is -7.52 dB, and to the dashed line, -11.14 dB.

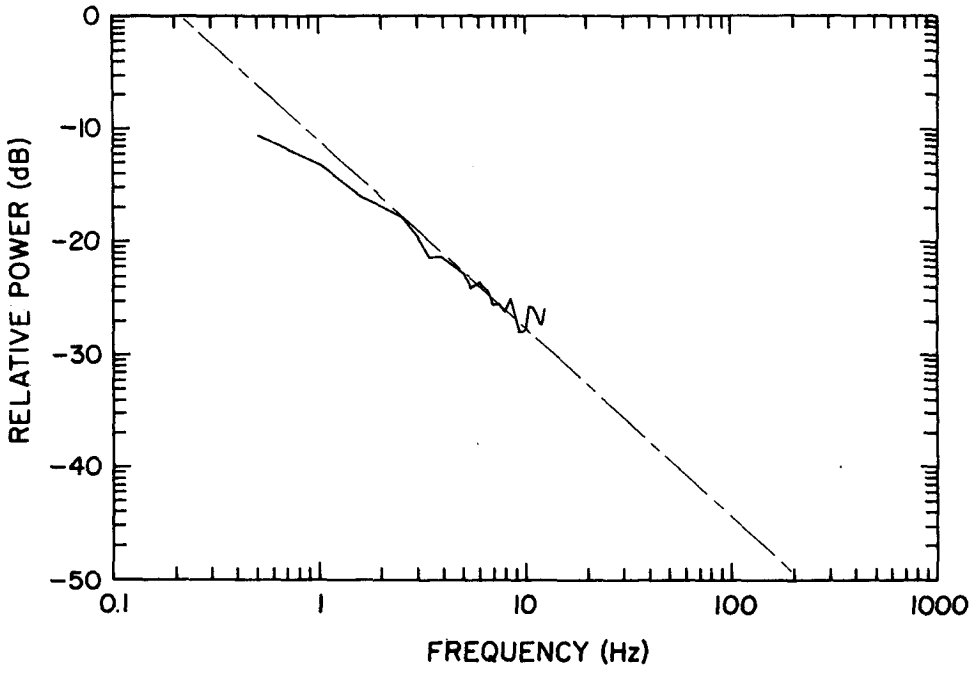

FIG. 6. Velocity power spectrum of the time series in Fig. 2 that is derived from laser velocimeter data. The fitted y intercept at 1 Hz is -11.06 dB.

less than 2 m depth of focus). The shear and turbulence contribution to the Doppler spectrum in Fig. 7 is then less than 1.1 m s^{-1} over a sample length of 17 m (1.5 m s^{-1} measured minus 0.4 m s^{-1} accounted for by known instrumental effects), but we do not have test data to separate this Doppler spectrum width into atmospheric and further instrumental contributions. A Doppler spectrum width of 1.1 m s^{-1} is only slightly larger than expected from the atmosphere at a scale of 17 m; recall that 1.1 m s^{-1} is the full width at half

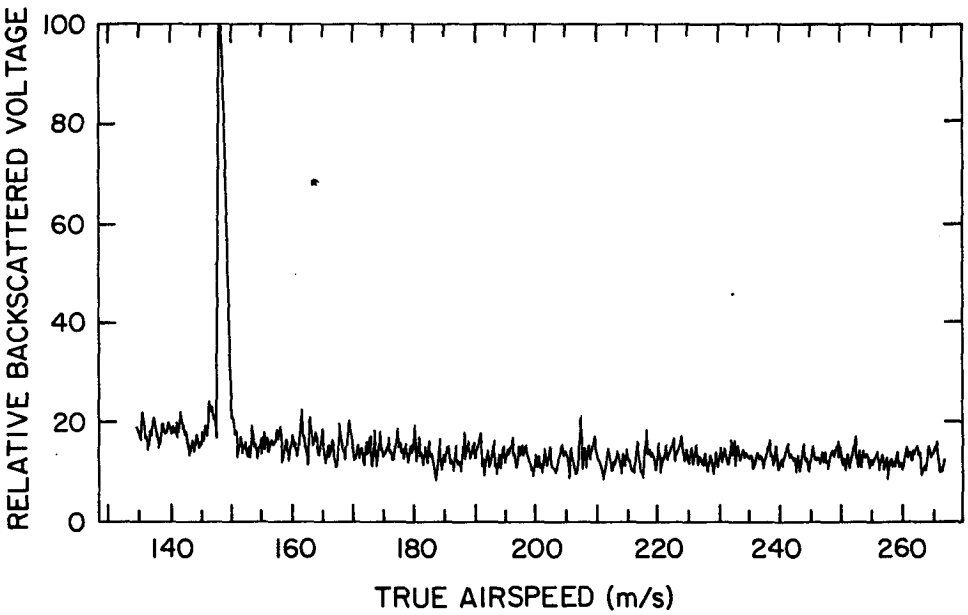

FIG. 7. Doppler voltage spectrum from the laser air motion sensor in clear air, focused 16 m ahead of the aircraft. The full width at half power of the spectrum is 1.5 m s^{-1}, and the ratio of peak power to rms fluctuations is approximately 36 dB.

power of the Doppler spectrum; the $1-\sigma$ width would be approximately 0.5 m s^{-1}. An idea of the expected contribution of turbulence to the Doppler width can be obtained from the pressure probe time series in Fig. 2, which has a variance of 2.89 (m s^{-1})^2. The portion of the turbulence spectrum of Fig. 5 from 9 Hz upward (corresponding to a wavelength of 17 m at 149 m s^{-1}) has a standard deviation of 0.3–0.5 m s^{-1}, depending on the outer scale assumed, using a $-5/3$ inertial subrange spectrum.

Figure 8 shows a narrower Doppler spectrum of 1.2 m s^{-1} FWHP. Although narrower in comparison to the previous spectrum, this asymmetric spectrum shows two distinct spectral peaks and considerable broadening below the 30% power level. This could be interpreted as two air parcels in the sample volume with different relative velocity components, but the fact that the data were taken near or at the edge of a cloud and that the spectrum is shaded to lower velocities from a peak of 150 m s^{-1} suggests a different interpretation.

2) Cloud effects

Werner et al. (1984) show that strongly scattering clouds and fog outside the focal volume of a cw Doppler lidar can have an influence on the Doppler spectrum. When the laser velocimeter is operating in clear air but with a cloud in the distance, far beyond the range to the sample volume, a Doppler spectrum with a double spectral peak is often observed. Figure 8 shows such a spectrum, and similar observations have been made with ground-based CO_2 Doppler lidars (Werner et al., 1984). The separation of the two peaks measures the difference between radial velocities near the cloud boundary and in the focal volume. Determining the sign of the velocity difference involves identifying the origin of the peaks (cloud or clear air). Although further work on identification is needed, promising techniques include determining the clear-air peak from closeness to an approximate (Pitot tube) airspeed indicator, from continuity in time, and by changing focal distance, where the cloud peak increases with increasing focal distance. This velocity difference probably has several causes. One is the influence of the cloud in modifying or diverting the environmental flow. Entrainment near the cloud boundary can also produce variability in the observed radial velocity.

Figure 9, from data taken in denser cloud than that for Fig. 8, shows even more shading to lower velocity although the peak of the Doppler spectrum is still at 149 m s^{-1} and the FWHP value is only 2.3 m s^{-1}. The attenuating effect of the cloud is seen in the smaller ratio of peak signal-to-baseline noise level in Fig. 9, compared to Fig. 7. The root structure in the spectrum caused by the cloud is below the 30% power level (measured from the average value of the baseline); the asymmetry, though visible on a voltage spectrum, results in a maximum difference between the speed at the peak of the spectrum and the mean of the spectrum of 0.1 m s^{-1}.

Work on the attenuation of CO_2 laser radiation in fog (Chimelis, 1982) is consistent with an attenuation of approximately 600 dB km^{-1} for a liquid water content of 1 g/m^3 and a linear relation between attenuation and liquid water content. The backscatter coefficient of a cumulus cloud is roughly 30 dB more than that of typical aerosols, based on an estimate of 20 dB more for cirrus (Post et al., 1982). With these backscatter/

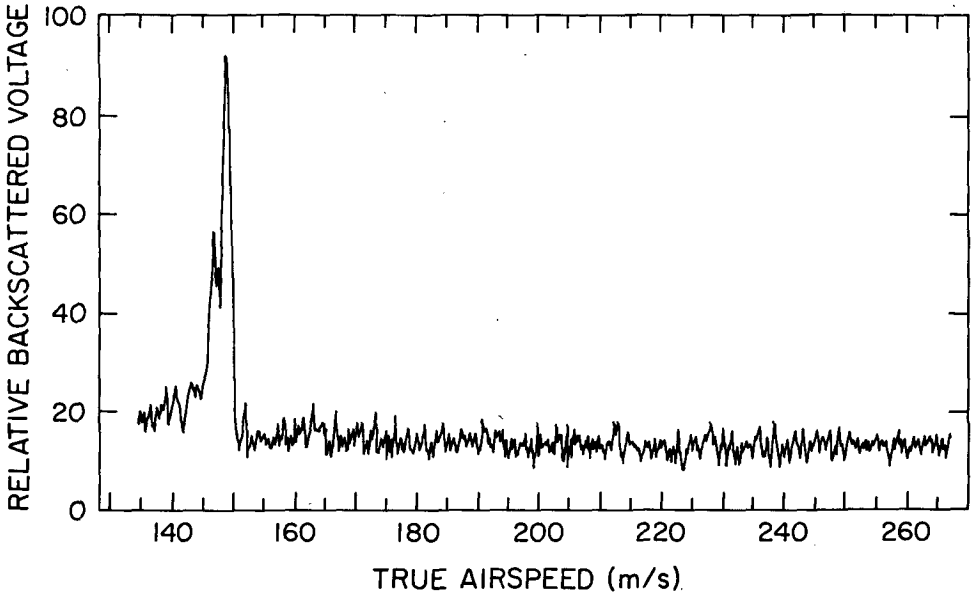

FIG. 8. As in Fig. 7 but with cloud ahead of the aircraft. The width of the spectrum is 1.2 m s^{-1}.

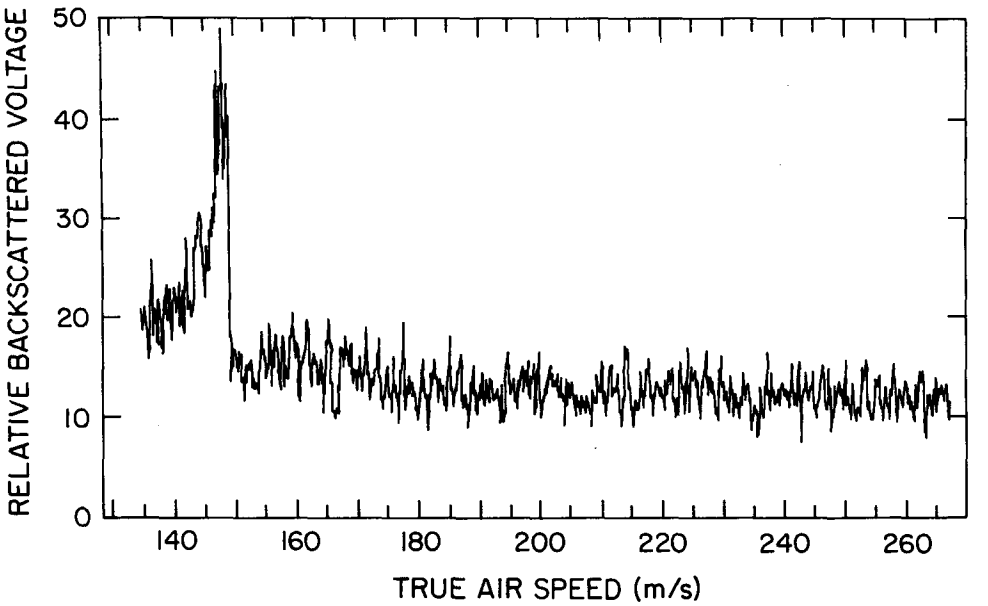

FIG. 9. As in Fig. 8 but in heavier cloud. The width of the spectrum is 2.3 m s^{-1}, and the difference between the speed at the peak of the spectrum and the first moment of the power spectrum is 0.1 m s^{-1}.

attenuation ratios and an allowable 10 dB degradation in SNR for cloud compared to aerosol data, we estimate a penetration depth of 200 m into a 0.2-g m^{-3} cloud.

Contributions to the Doppler spectrum at lower velocity come from the region near the aircraft where the relative air motion is slowed by interference from the fuselage. When operating in cloud, it appears that the airspeed measurement should be made at the peak of the skewed spectrum rather than from the mean, which is appropriate for clear air.

3) SIGNAL-TO-NOISE RATIO

Without an independent measure of the aerosol backscatter coefficient (which was not available for the experiment), it is not possible to calculate an accurate expected SNR. The experimental SNR from the ratio of peak signal voltage to rms (fluctuating) noise in Fig. 7 is approximately 70, which is a power SNR of 4900, i.e., 36 dB. The voltage peak is determined with respect to frequency for a spectrum that is the average over many independent realizations of the Doppler spectrum, as is the case in Fig. 7. The voltage at the peak of the spectrum and the noise voltage are both functions of the bandpass (i.e., resolution) of the spectrum analysis system, but if the bandpass of the analyzer (approximately 80 kHz in this case) is narrower than the bandwidth of the Doppler signal (420 kHz in this case), then the *ratio* of signal peak voltage to rms noise voltage is independent of analyzer bandpass.

The SNR expected by (7) is 38.7 dB, based on the following estimates for the experimental parameters. The backscatter coefficient in the boundary layer in England in the summer is assumed to be 1×10^{-7} m^{-1} sr^{-1}. The transmitted power is 2 W, and heterodyne, speckle and optical efficiency, respectively, are estimated as 0.95, 0.5 and 0.7 (Foord et al., 1983). Speckle efficiency is discussed in detail by Foord et al. (1983) and involves the ratio of the receiver aperture area to the area of a coherent wavefront. Another way of looking at speckle efficiency involves the spatial overlap of the diffraction-limited focal volumes of the receiver and transmitter optics. The detector quantum efficiency is approximately 0.4, and the signal bandwidth is 1/(2.4 μs) or 420 kHz from (8). Using these values in (2) and (7) gives a detector SNR of 23.6 dB. Each individual spectrum of 25 μs contains 25/2.4 independent samples, and 100 such spectra are averaged in Fig. 7 for a total integration time of 2.5 ms. The square root of this averaging factor adds 15.1 dB to the expected single-sample SNR estimate, for an overall expected SNR in Fig. 7 of 38.7 dB. The remarkable agreement between estimated and experimental SNRs is much better than should be expected legitimately given the uncertainties inherent in estimating the backscattering coefficient.

It is clear that the spectrum in Fig. 7 has an adequate SNR to make an estimate of mean velocity in the sample volume to within 10% of the spectrum width (i.e., an uncertainty of ± 0.1 m s^{-1}, even with a system not specifically designed for high-resolution gust probe use. Theoretically [section 2a, (3)], the uncertainty is even less. Better resolution in the spectrum display would make it easier to visualize the achievable velocity accuracy.

The accuracy achieved in estimating the mean can be less than the resolution of the spectrum analyzer (FWHP of 0.3 m s^{-1} in this case) if the SNR is adequate. Accuracy should not be confused with resolution in the sense of resolving the existence of two regions in the sample volume with slightly differing mean velocities. Velocity resolution in this sense is limited to the spectrum analyzer resolution.

4. Conclusions

a. Performance

A single-component laser air motion sensor performs well in comparison with a conventional 5-port pressure difference gust probe, up to a data rate of 10 s^{-1} in actual airborne tests. The SNR achieved with the instrument using an integration time of 2.5 ms (but a data rate of only 10 s^{-1} due to processor limitations) is sufficient to make estimates of the mean velocity in the sample volume to less than ± 0.1 m s^{-1} uncertainty for the longitudinal component of relative air motion, and it agrees with theory. Velocity spectra from the time series of velocity measured by the two techniques are very similar up to the 10-Hz cutoff of the optical data processing system, so the laser air motion sensor is shown to have the same response to turbulence (in the longitudinal component) as a pressure-difference probe up to 10 Hz.

The laser air motion sensor operates in cloud with a slightly degraded SNR caused by optical attenuation countered by increased backscatter. In cloud, it is important to use the peak of the Doppler spectrum rather than the mean to estimate the velocity.

In addition to adequate comparative performance, the laser air motion sensor has a number of advantages over instruments based on conventional techniques that are only partly illustrated by the experiment. Figures 1 and 2 suggest the advantage of a calibration based only on physical parameters and not on empirical calibration and correction. Comparing Fig. 7 with Figs. 8 and 9 show that flow distortion is of no concern in clear air. Flow distortion effects are present for measurements made in cloud, but these can be corrected by proper data processing. The figures do not address the advantage of freedom from attenuation and crosstalk in measurement of turbulent velocity covariances possessed by the optical probe by virtue of operating outside of flow distortion induced by the fuselage. Freedom of an optical probe from precipitation, icing and resonance effects has not yet been established experimentally, but is reasonable to expect.

b. Further study and experiment

The feasibility of obtaining three turbulent components of air motion from a conically scanned laser velocimeter is analyzed by Kristensen and Lenschow (1986). Methods to increase the spatial frequency response of a laser air motion sensor, for example by using three intersecting beams, require study. The relation between turbulence and instrumental contributions to the Doppler spectrum width, explored in section 3c (1), is not yet clearly established.

Operation of a laser air motion sensor in precipitation and icing and aboard a propeller-driven aircraft should help determine the adequacy of the technique in harsh environments. An experimental test of the ability of a conical scan to produce data from which three components of air motion can be derived is a key test. Any alternative optical configurations that appear promising from analytical studies deserve investigation. The effects of cloud on the Doppler spectra as a function of range to the sample volume, liquid water content and particle size spectrum remain to be explored.

Acknowledgments. The authors gratefully acknowledge the professional assistance of the RAE/Bedford staff. John Cannell provided guidance and information during the flight test portion of the research. David Bull and Graham Foster's aid in computer processing of the data at RAE was essential in producing the results shown in this paper.

REFERENCES

Bilbro, J., G. Fichtl, D. Fitzjarrald, M. Krause and R. Lee, 1984: Airborne Doppler lidar wind field measurements. *Bull. Amer. Meteor. Soc.*, **65**, 348–359.

Boyd, R. W., 1983: *Radiometry and the Detection of Optical Radiation.* Wiley, 254 pp.

Browning, K. A., and R. Wexler, 1968: The determination of kinematic properties of a wind field using Doppler radar. *J. Appl. Meteor.*, **7**, 105–113.

Cannell, J., R. Foord, J. M. Vaughan and A. Woodfield, 1983: The RSRE/RAE laser true airspeed system (LATAS). *Second Topical Meeting on Coherent Laser Radar,* Aspen, Opt. Soc. Am., WA4-1–WA4-4.

Caughey, S. J., and J. C. Kaimal, 1977: Vertical heat flux in the convective boundary layer. *Quart. J. Roy. Meteor. Soc.*, **103**, 811–815.

Chimelis, V., 1982: Extinction of CO_2 laser radiation by fog and rain. *Appl. Opt.*, **21**, 3367–3372.

Dickson, D. H., and J. E. Ottesen, 1980: Helicopter remote wind sensor flight test. U.S. Army ERADCOM Tech. Rep. ASL-TR-0051, Atmospheric Sciences Laboratory, White Sands Missile Range, 41 pp.

Eilts, M. D., R. J. Doviak and A. Sundara-Rajan, 1984: Comparison of winds, waves and turbulence as observed by airborne lidar, ground-based radars and instrumented tower. *Radio Sci.*, **19**, 1511–1522.

Fitzgerald, J. W., 1984: Effect of relative humidity on the aerosol back-scattering coefficient at 0.694- and 10.6-μm wavelengths. *Appl. Opt.*, **23**, 411–418.

Foord, R., R. Jones, J. M. Vaughan and D. V. Willetts, 1983: Precise comparison of experimental and theoretical SNRs in CO_2 laser heterodyne systems. *Appl. Opt.*, **23**, 3787–3795.

Gossard, E. E., and R. G. Strauch, 1983: *Radar Observations of Clear Air and Clouds.* Elsevier, 292 pp.

Keeler, R. J., 1980: Doppler estimator error for coherent CO_2 lidar. *First Topical Meeting on Coherent Laser Radar,* Aspen, Opt. Soc. Am., WA3-1–WA3-4.

——, and R. J. Serafin, 1983: An airborne coherent lidar for turbulence measurement. *Second Topical Meeting on Coherent Laser Radar,* Aspen, Opt. Soc. Am., MC6-1–MC6-3.

——, ——, J. M. Vaughan and A. Woodfield, 1984: Comparison of turbulence measurements from an airborne coherent lidar and a differential pressure gust probe. *Proc. of 12th Int. Laser Radar Conf.*, Aix-en-Provence, Opt. Soc. Am., 348–352.

Kristensen, L., and N. O. Jensen, 1979: Lateral coherence in isotropic turbulence and in the natural wind. *Bound.-Layer Meteor.*, **17**, 353–373.

——, and D. H. Lenschow, 1986: An airborne laser air motion sensing system. Part II: Criteria for design. *J. Atmos. Oceanic Technol.*, **4**, 126–136.

Lee, R. W., and K. A. Lee, 1980: A polypulse-pair signal processor for coherent Doppler lidar. *First Topical Meeting on Coherent Laser Radar*, Aspen, Opt. Soc. Am., WA2-1–WA2-4.

Lenschow, D. H., 1986: Aircraft measurements in the boundary layer. *Probing the Atmospheric Boundary Layer*, D. H. Lenschow, Ed., Amer. Meteor. Soc., Boston, 39–56.

Lhermitte, R. M., and D. Atlas, 1961: Precipitation motion by pulse Doppler. *Preprints, Ninth Weather Radar Conf.*, Kansas City, Amer. Meteor. Soc., 218–223.

Muñoz, R. M., H. W. Mocker and L. Koehler, 1974: Airborne laser Doppler velocimeter. *Appl. Opt.*, **13**, 2890–2898.

Parkinson, B. W., and S. W. Gilbert, 1983: NAVSTAR: Global positioning system—ten years later. *Proc. IEEE*, **71**, 1177–1186.

Post, M. J., 1978: Experimental measurements of atmospheric aerosol inhomogeneities. *Optics Letters*, **2**, 166–168.

——, 1984: Aerosol backscattering profiles at CO_2 wavelengths: the NOAA data base. *Appl. Opt.*, **23**, 2507–2509.

Schwiesow, R. L., 1986: Lidar measurement of boundary-layer variables. *Probing the Atmospheric Boundary Layer*, D. H. Lenschow, Ed., Amer. Meteor. Soc., 139–162.

——, F. F. Hall, R. A. Richter and T. R. Lawrence, 1982: Aerosol backscattering profiles at lamda = 10.6 μm. *Appl. Opt.*, **21**, 2442–2446.

——, R. E. Cupp, M. J. Post and R. F. Calfee, 1977: Coherent differential Doppler measurements of transverse velocity at a remote point. *Appl. Opt.*, **16**, 1145–1150.

——, ——, V. E. Derr, E. W. Barrett, R. F. Pueschel and P. C. Sinclair, 1981b: Aerosol backscatter coefficient profiles measured at 10.6 μm. *J. Appl. Meteor.*, **20**, 184–194.

Werner, C., F. Kopp and R. L. Schwiesow, 1984: Influence of clouds and fog on LDA wind measurements. *Appl. Opt.*, **23**, 2482–2484.

Woodfield, A. A., and J. M. Vaughan, 1983: Airspeed and wind shear measurements with an airborne CO_2 cw laser. *Int. J. Aviation Safety*, **1**, 207–224.

Wyngaard, J. C., L. Rockwell and C. A. Friehe, 1985: Errors in the measurement of turbulence upstream of an axisymmetric body. *J. Atmos. Oceanic Technol.*, in press.

Yariv, A., 1985: *Optical Electronics*, 3rd ed. Holt, Reinhart & Winston, 566 pp.

Zrnić, D. S., 1979: Estimation of spectral moments for weather echos. *IEEE Trans. on Geosci. Electron.*, **GE-17**, 113–128.